2016

From imagery to ecology: Leveraging time series of all available Landsat observations...

Remote Sensing in Ecology and Conservation
Open Access
ZSL LET'S WORK FOR WILDLIFE

ORIGINAL RESEARCH

From imagery to ecology: leveraging time series of all available Landsat observations to map and monitor ecosystem state and dynamics

Valerie J. Pasquarella[1], Christopher E. Holden[1], Les Kaufman[2,3] & Curtis E. Woodcock[1]

[1]Department of Earth & Environment, Boston University, Boston, Massachusetts 02215
[2]Department of Biology, Boston University, Boston, Massachusetts 02215
[3]Moore Center for Science and Oceans, Conservation International, 2011 Crystal Drive, Arlington, Virginia 22202

Keywords
Ecosystem dynamics, ecosystem structure, land cover, Landsat, time series, vegetation mapping

Correspondence
Valerie J. Pasquarella, Department of Earth & Environment, Boston University, Boston, MA 02215. Tel: +1 617-353-2525; Fax: +1 617-353-8399;
E-mail: valpasq@bu.edu

Funding Information
This work was funded in part by the US Forest Service (13-CR-11221638-146), the US Geological Survey (G12PC00070) and NASA (NNX13AP42).

Editor: Harini Nagendra
Associate Editor: Kate He

Received: 7 April 2016; Revised: 17 June 2016; Accepted: 5 July 2016

doi: 10.1002/rse2.24

Abstract

With over 30 years of directly comparable Landsat satellite observations now freely available, and new imagery being added to the Landsat archive every day, Landsat time series analysis affords novel opportunities for ecosystem mapping, environmental monitoring and comparative ecology. This study presents a series of data-driven examples that illustrate the potential of using Landsat time series to further the study of land cover characterization, vegetation phenology and landscape dynamics. Our goal is to showcase how ecosystem properties and dynamics manifest in the Landsat data record, laying the foundation for better integration of remote sensing and ecology using Landsat time series. Our results suggest that time series provide valuable information on ecosystem cover, use and condition that could advance understanding of ecosystem function, resilience and dynamics. We have only just begun to understand how to use the complete record of Landsat observations for the study of ecology, and we hope this work will encourage future studies on quantifying and analyzing relationships between time series data, ecosystems and ecological processes.

Introduction

Landsat imagery has been used to map and monitor Earth's ecosystems since the early 1970s (Cohen and Goward 2004; Lauer et al. 1997; Wulder et al. 2008), yet we have only just begun to utilize the complete Landsat record to study long-term large-scale ecosystem dynamics (Wulder et al. 2012; Hansen and Loveland 2012; Kennedy et al. 2014). Prior to a 2008 change in data policy (Woodcock et al. 2008), image costs and computing capacity limited Landsat-based analyses to a relatively small number of carefully selected images (Coppin et al. 2004; Kennedy et al. 2014). Today, all new and archived Landsat images held by the United States Geological Survey (USGS) are available for free download in a variety of user-friendly formats, making Landsat data more accessible than any time in the history of the Landsat program (Loveland and Dwyer 2012; Wulder et al. 2015). With free and open access to the Landsat archive, it is finally possible to leverage the full temporal dimension of the Landsat record to support the study of ecology and biodiversity (Kennedy et al. 2014; Turner et al. 2015).

Since the opening of the Landsat archive, many new Landsat time series-based approaches have emerged. Landsat time series data have been successfully used to map both abrupt and gradual forest change (e.g. Huang et al. 2010; Kennedy et al. 2010; Vogelmann et al. 2012;

Hansen et al. 2013; Kim et al. 2014; Hermosilla et al. 2015) and detect changes in wetland ecosystems (Kayastha et al. 2012; Fickas et al. 2015), yet many analyses still use only snapshots from the Landsat record, relying on best-available anniversary date imagery or annual composites to monitor complex ecosystem dynamics. A handful of pioneering studies have employed time series of all available observations for individual pixels to improve characterization of land cover types (Zhu and Woodcock 2014), map abrupt change such as forest clearing and development (Zhu et al. 2012b; Brooks et al. 2014; Zhu and Woodcock 2014; DeVries et al. 2015a), and monitor deciduous forest phenology (Melaas et al. 2013). However, research utilizing the extensive record of Landsat observations is still in its infancy. As remote sensing analysis moves from a relatively static, bi-temporal view of change toward a more continuous view of ecosystem dynamics (Kennedy et al. 2014), there is a critical need for data-driven examples that establish the utility of the full Landsat temporal domain.

In this study, we present examples that illustrate the potential of using Landsat time series to map and monitor a wide variety of ecosystem properties and processes. Building on existing conceptual frameworks for using remotely sensed imagery for ecosystem monitoring (Coppin et al. 2004; Kennedy et al. 2014), these examples are grouped into two broad categories: (1) *seasonal profiles*, where time series of all available observations are used to characterize intra-annual variability, i.e. phenology; and (2) *temporal trajectories*, which characterize changes in state or trends in ecosystem condition above and beyond the range of normal seasonal variability. We do not attempt to quantify the patterns observed; rather, our goal is to showcase how ecosystem properties and dynamics manifest in the Landsat data record, laying the foundation for better integration of remote sensing and ecology via Landsat time series applications.

Materials and Methods

Our approach for downloading, processing and visualizing time series of all available Landsat imagery is generalizable across Landsat sensors and scenes, making it possible to assemble time series data for practically anywhere on Earth. Here we briefly describe the images we select, the spectral transformations we apply, and the basic approaches to time series visualization and interpretation that we use throughout the remainder of this paper.

Imagery

For each of our study sites, we acquired all available images from Landsat 4 (1982–1993), Landsat 5 (1984–2011) and Landsat 7 (1999–present) that were processed to a level-one terrain corrected (L1T) product and have cloud cover of less than 80%. L1T products are georeferenced, terrain-corrected and radiometrically calibrated across Landsat sensors, enabling direct comparison of individual pixels over time (Loveland and Dwyer 2012; Markham and Helder 2012). We excluded L1T images with greater than 80% cloud cover because these images may be less accurately georeferenced and image registration is important for time series analysis. The remaining L1T images were processed to correct for atmospheric conditions and to identify and mask clouds and cloud shadows by the USGS EROS Science Processing Architecture (ESPA) (DeVries et al. 2015; DeVries et al. 2015a). This preprocessing to cloud-masked surface reflectance Landsat data, once difficult to accomplish as an individual, is now easily available from the USGS as a Climate Data Record.

Tasseled Cap transformation

For each image, we applied the Tasseled Cap (TC) transformation to reduce the dimensionality of Landsat's six optical spectral bands into three orthogonal indices that are easier to visualize and interpret. The design of the TC transformation specifically emphasizes inherent data structures that capture key physical properties of vegetated systems that can be compared both within and across scenes (Crist and Kauth 1986). TC Brightness (TCB) generally captures variation in overall reflectance, or something akin to albedo; TC Greenness (TCG) captures variability in green vegetation; and TC Wetness (TCW) responds to a combination of moisture conditions and vegetation structure (Crist and Cicone 1984; Cohen and Spies 1992). We calculate TCB, TCG and TCW for each pixel using the band weightings provided by Crist (1985) (Fig. 1).

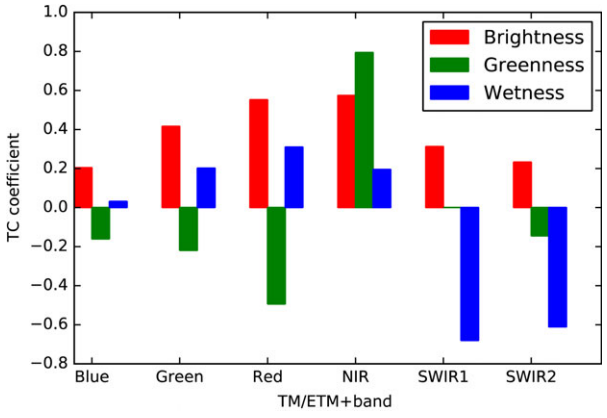

Figure 1. Tasseled Cap (TC) coefficients for Brightness (TCB), Greenness (TCG) and Wetness (TCW) by band, *adapted from Crist 1985; Cohen and Spies 1992.

Time series visualization

Time series data may be visualized in a variety of ways to achieve different analysis and interpretation goals (Fig. 2). In terms of organization, time series can be ordered by sequential date, e.g. chronologically ordered from August 1982 to September 2014 (Fig. 2A and C), or based on the Day-Of-Year (DOY) of image acquisition, i.e. from DOY 1 (January 1) to DOY 365 (December 31) (Fig. 2B and D). Sequential date plots tend to emphasize long-term trends in ecosystem condition, whereas DOY plots emphasize intra-annual variability and vegetation phenology, and different colors or symbols can be applied to emphasize underlying temporal patterns. Throughout the remainder of this paper, we use various combinations of the plots and symbology shown in Figure 2 to present time series of TCB, TCG and TCW.

Time series interpretation

Field observations and other reference data are essential for the interpretation of the complex temporal dynamics observed in time series data (Kennedy et al. 2014). For this study, we drew on reference data from many domains to identify and interpret time series examples. In some cases, existing local, regional and global land cover datasets were used to provide general descriptions of land surface conditions. Other examples were selected using site-specific knowledge, ranging from monitoring plot data to previously published research to narrative histories provided by local land managers. In all cases, high-resolution Google Earth (GE) imagery was used to corroborate reference information, and selected GE images have been included for most examples to aid in the interpretation of time series data while also highlighting the limitations of using infrequent single-date snapshots to assess complex temporal dynamics.

Results

The examples that follow illustrate how the Landsat record can be used in characterizing and analyzing both stable and changing ecosystems. We begin with time series that highlight intra-annual variability in land surface reflectance, exploring differences in phenology across forest types and land cover gradients. We then move to time series that capture changes in land cover and ecosystem state, including cyclic changes, abrupt changes, disturbance-recovery and gradual changes.

Seasonal profiles

The production of thematic land cover maps has long been one of the most prevalent uses of remote sensing imagery (e.g. Cihlar 2000; Cohen and Goward 2004). Historically, Landsat-based land cover classification has largely relied on the spectral properties of pixels or patches at a single point in time (e.g. Walsh 1980; Lu and Weng 2005) or a limited set of multi-season observations (e.g. Wolter et al. 1995; Zhu et al. 2012a). However, time series data support leveraging the temporal domain for improved land cover classification (Gómez et al. 2016). The examples in this section highlight how temporal variability in reflectance can be used to better characterize land cover types.

Forest phenology

Prior to the opening of the Landsat archive, efforts to map forest communities relied on single-date images or sets of images that maximized phenological differences among forest types (e.g. Reese et al. 2002). We use 12 pixel-level examples drawn from study areas in Colombia, Vietnam, Massachusetts (USA), and Finland to illustrate seasonal variability in the full spectral-temporal signatures of select forest types. Figure 3 shows seasonal variability in TCG for these 12 sites. As would be expected, TCG profiles for the humid tropical forests of Colombia, (A) and (B), and tropical mangroves of Vietnam, (C), show little intra-annual variability, whereas TCG profiles for examples from Massachusetts and Finland, (D)–(L), exhibit more pronounced phenological patterns. Deciduous species such as oak, hickory, beech and birch, (D)–(F), (L), have a high seasonal amplitude in TCG, with TCG profiles capturing distinct leaf-on, leaf-off and transitional periods. Needle-leaf forests such spruce, fir, pine and hemlock, (G)–(K), also exhibit seasonal changes in TCG, but variability is consistently lower.

TCW profiles for the same 12 examples are shown in Figure 4. Again, profiles for the tropical forests are relatively a-seasonal, but the TCW profile of the inundated mangroves, (C), is consistently higher ('wetter') than the profile of the upland humid tropical forest examples from Colombia, (A) and (B). Similarly, the profiles of temperate conifer and humid tropical forests are relatively flat by comparison, with more limited intra-annual variability. The seasonal variability in TCW is more apparent in the profiles of deciduous forest communities, which exhibit a distinct plateau during the leaf-on period, with lows during the onset of spring and onset of autumn. While TCW has been shown to correlate strongly with forest structural attributes and improve classification of both broadleaf deciduous and needle-leaf species (Cohen and Spies 1992; Cohen et al. 2001; Dymond et al. 2002; Healey et al. 2005), the distinct seasonal patterns in TCW shown here are, to the best of our knowledge, reported for the first time in this study.

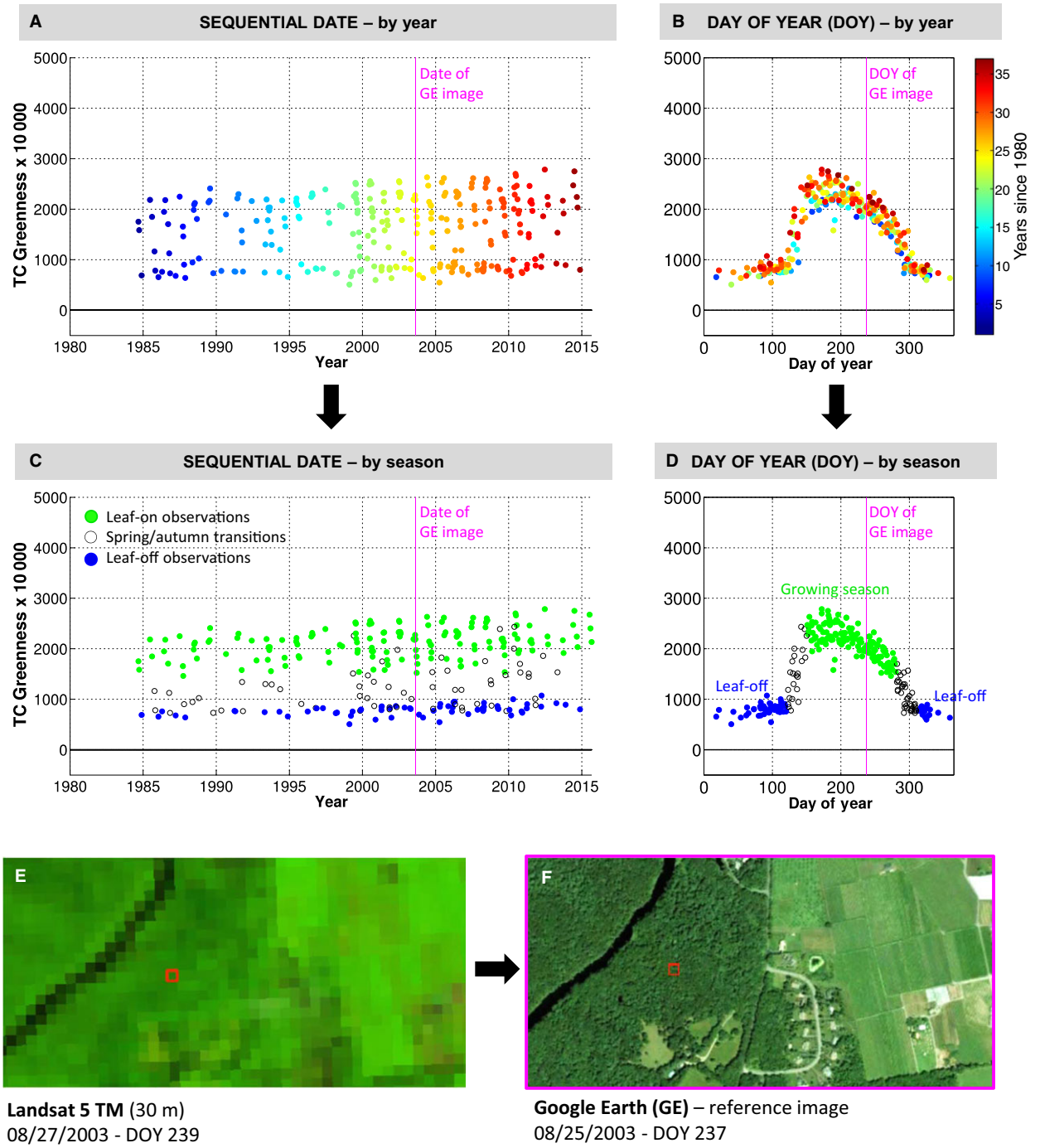

Figure 2. Visualizing and interpreting Landsat time series. Plots A–D show four visualizations of a Tasseled Cap Greenness time series that includes all available high-quality Landsat TM/ETM+ observations for a single pixel located in a temperate deciduous forest (MA, USA). Sequential date plots (A and C) order observations chronologically (with year ticks set to January 1 of each year), whereas Day of Year (DOY) plots (B and D) show observations ordered by the DOY of image acquisition. Observations are color-coded in two different ways. Observations in plots (A) and (B) are color-coded by year of acquisition, whereas observations in plots (C) and (D) are color-coded based on season of acquisition. Vertical lines indicate the date/DOY of the high-resolution Google Earth image (F), which captures late summer leaf-on conditions. A Landsat image for a comparable date (E) is included to highlight differences in resolution. This figure serves as a template for interpretation of all figures that follow.

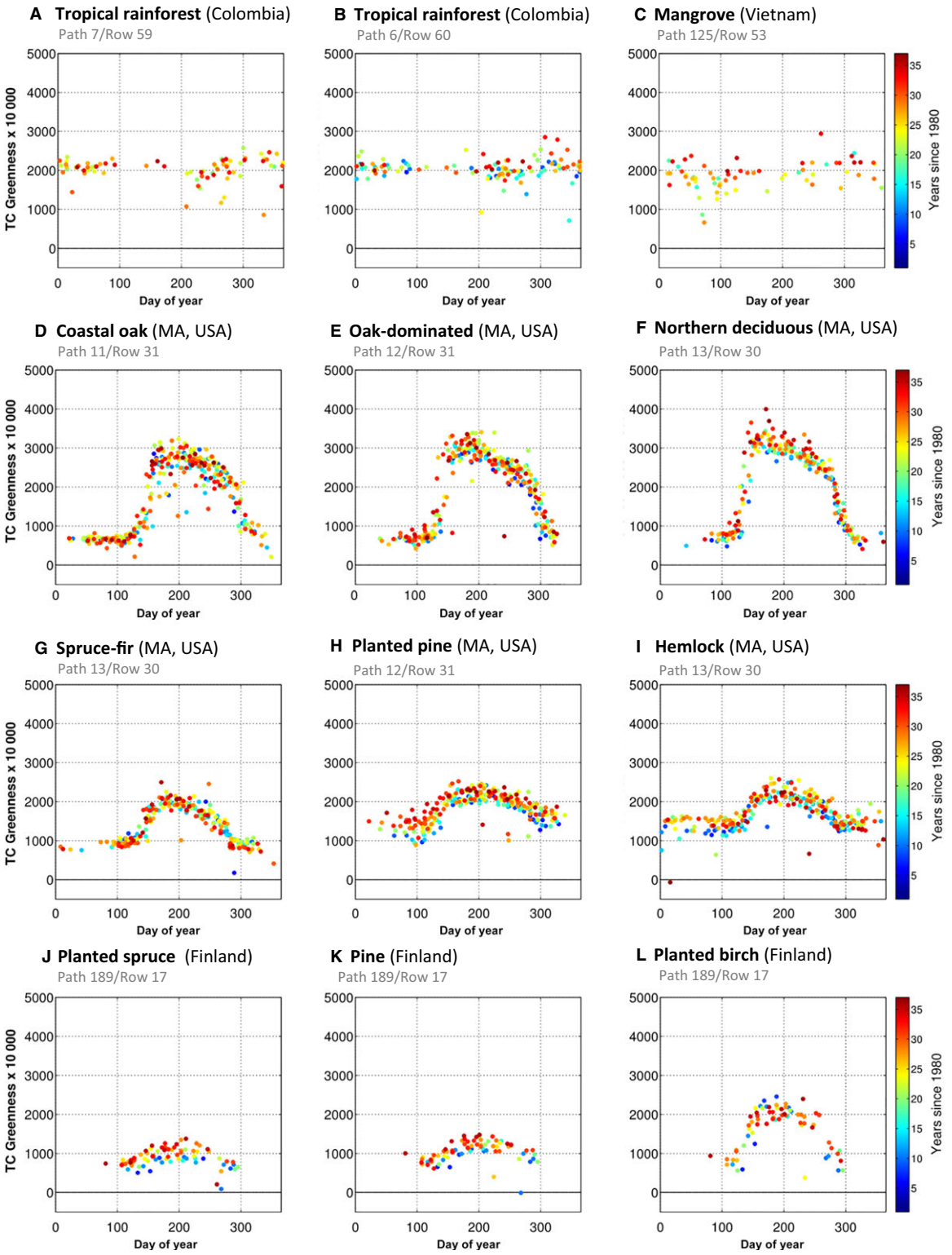

Figure 3. Seasonal Tasseled Cap Greenness (TCG) profiles for 12 forested sites. Profiles show all available high-quality Landsat observations for a single pixel. Forest types have been labeled according to best-available reference data, and the World Reference System 2 (WRS2) path and row of the corresponding Landsat scene is provided for reference. Note both seasonal differences in TCG, as well as differences in observation density across sites, forest types and latitudes.

Wetland gradients

Wetlands have been notoriously difficult to characterize using moderate resolution optical instruments like Landsat due to high image-to-image variability and land surface heterogeneity (Özesmi and Bauer 2002; Adam et al. 2009). To determine how the temporal dimension of Landsat data might be used to better distinguish among wetland states, we generated TCB, TCG and TCW profiles for examples of three common wetland types: open water, seasonal emergent wetland and shrub swamp (Cowardian & Meyers 1974).

The seasonal profiles of these different wetland types, which have been drawn from our Eastern Massachusetts study area, capture distinct seasonal and structural characteristics (Fig. 5). Persistent open water systems like lakes and ponds have near-zero TCB, TCG and TCW values throughout the year, whereas both emergent (herbaceous-dominated) wetlands and woody shrub swamps show greater seasonal variability in TCB and TCG, driven by seasonal changes in vegetation. Furthermore, shrub swamps have asymmetrical profiles subtly resembling those of deciduous forests, whereas the profiles of the emergent wetland are more symmetric. These results suggest that the shape of the seasonal reflectance profile, particularly the intra-annual variability and skewness, will provide important clues as to the vegetated and hydrologic conditions of complex wetland ecosystems.

Urban gradients

Moderate resolution sensors like Landsat are unable to resolve fine-scale urban characteristics such as building type and transportation infrastructure (Jensen and Cowen 1999; Cadenasso et al. 2007), but spectral-temporal signatures can still aid in charactering mixtures of built and vegetated surfaces (e.g. Ridd 1995). To investigate the spectral-temporal variability in urbanized areas, we generated TCB, TCG and TCW profiles for three representative pixels from the greater Boston area with varying degrees of impervious surface/building coverage (Fig. 6). Though 'urban' spectral-temporal signatures would be expected to vary as a function of local landscape conditions and heterogeneity of impervious surface cover, we consider simple combinations of impervious and forest land cover for the sake of illustration.

As these examples show, areas covered completely by impervious materials have relatively flat seasonal profiles for TCB, TCG and TCW, with any seasonal pattern likely due to change in sun angle throughout the year. When just a small fraction of vegetation is present, the seasonal profiles exhibit a more pronounced seasonal signal, and in a wooded suburban area, the seasonal profiles appear to approach those of a deciduous forest, with the effects of canopy phenology far outweighing those of impervious surfaces. These spectral-temporal profiles may provide insights into complex sub-pixel mixtures and aid in improved mapping of human-dominated landscapes.

Temporal trajectories

In the preceding examples, we focused on pixels where land cover has remained relatively stable over the observation period so we could clearly visualize seasonal patterns and use these to enhance discrimination. In this section, we turn our attention to locations that have undergone some form of land cover change or ecological transition in the past 30 years. We have organized these examples based on their underlying inter-annual functional forms described by Kennedy et al. (2014): *cyclic functions, abrupt change, disturbance-recovery trajectories* and *trends*. For each example, we include both sequential date and DOY plots in select TC components to emphasize how Landsat time series data capture changes in both seasonal and inter-annual patterns and dynamics. All the examples are from our Eastern Massachusetts study area, where our interpretations benefit from dense time series data, a relatively large number of GE historical images, and a wealth of local ecological knowledge.

Cyclic trajectories

Cyclic functions are usually thought of in relation to seasonal dynamics, but they can also result from inter-annual changes in ecosystem state related to sociological, biophysical or climatological cycles. For example the TC trajectories and profiles in Figure 7 capture cyclic dynamics of a shifting tidal inlet at Mass Audubon's Allens Pond Sanctuary (Westport, MA). Tidal dynamics drive the movement and sealing of tidal inlets (FitzGerald et al. 2002), but at Allens Pond, a local organization intervenes and opens a new channel every 4–5 years to ensure continued exchange between the ocean and adjacent salt marsh. At the pixel scale, this results in a cyclic change in reflectance as the inlet moves along the beach producing brief (1–3 month) shifts from sand to water. Interestingly, though not surprisingly, the TCB and TCW trajectories exhibit similar but opposite responses to the periodic change in state, whereas TCG exhibits no response, as there is no vegetation present at any time. Though this inlet example is one of the first and only multi-year cyclic trajectories we have investigated, we might expect to find similar behavior in places that experience desert blooms (e.g. Dall'Olmo and Karnieli 2002) and systematic crop rotations.

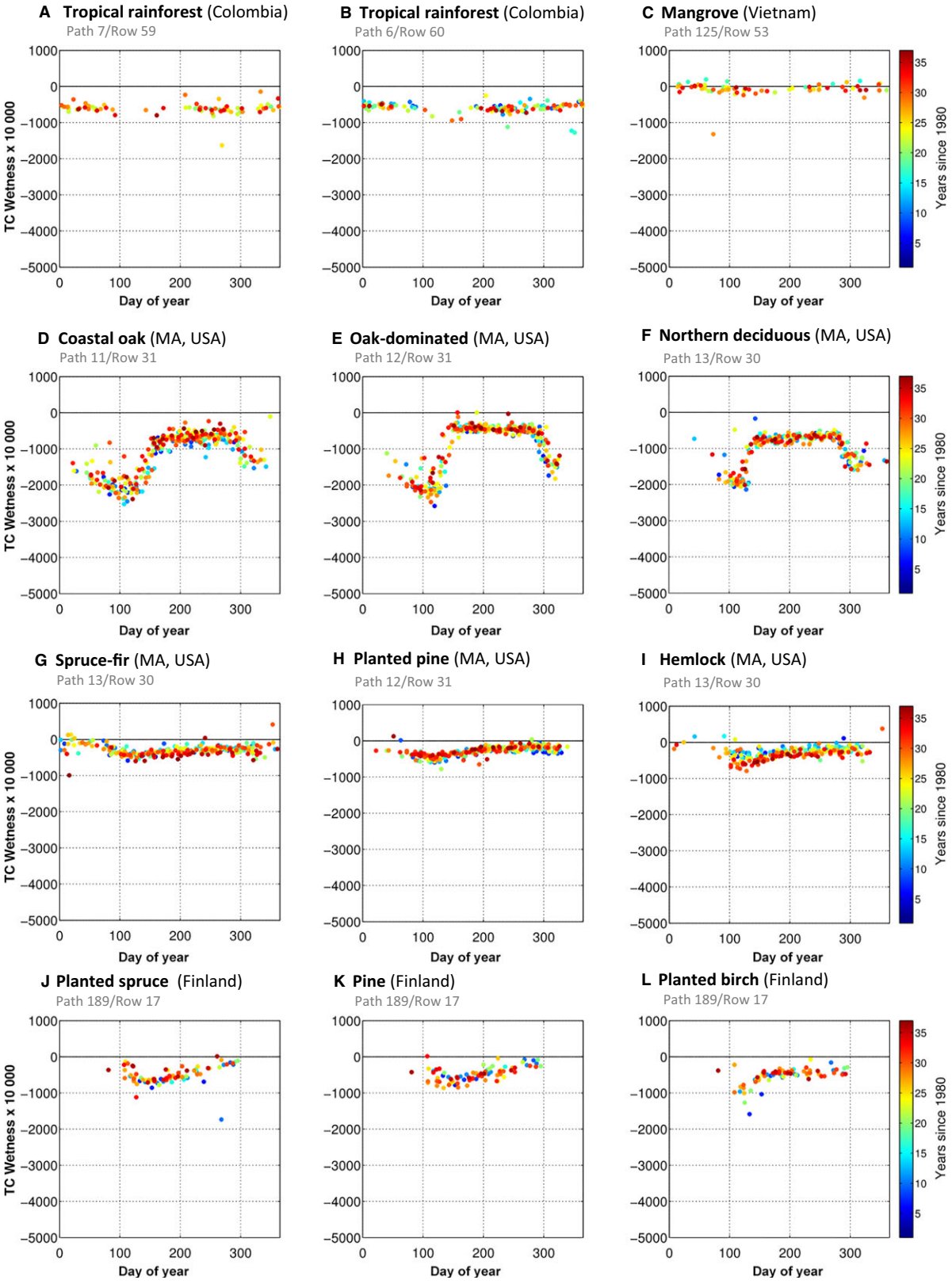

Figure 4. Seasonal Tasseled Cap Wetness (TCW) profiles for 12 forested sites. Profiles show all available high-quality Landsat observations for a single pixel. Forest types have been labeled according to best-available reference data, and the WRS2 path and row of the corresponding Landsat scene is provided for reference. Note both seasonal differences in TCW, as well as differences in observation density across sites, forest types and latitudes.

Abrupt, persistent changes in state

Abrupt shifts occur in ecosystems of all kinds (Folke et al. 2004), and fit well with the long-standing remote sensing paradigm of bi-temporal change detection. The temporal trajectory of an abrupt change in state is characterized by a step-function with a clear break point between metastable 'before' and 'after' conditions (Kennedy et al. 2014), and persistent abrupt changes tend to exhibit distinct seasonal profiles with little blending/overlap.

Abrupt changes can be associated with severe weather events, landslides, fire, flood, tsunami and volcanic or tectonic activity, but sustained changes in land surface cover and condition are most often linked to human activities. Time series that capture obvious human-induced changes in vegetation state and condition are relatively common. For example Figure 8A shows a time series for a forested area that was cleared to create a golf course. This abrupt shift in state is visible in GE imagery, as well as in the sequential date plot, which captures a rapid shift in the seasonal amplitude of TCG following the transition from forest to managed turf. Differences in the seasonal signals of the forest and the golf course are observed in the DOY plot, with the golf course exhibiting higher and less variable TCG throughout the year.

Time series data also reveal interesting dynamics in built environments. We have observed many urban sites that exhibit abrupt breaks between highly stable reflectance conditions. In some cases, GE imagery suggests these breaks correspond to a change in roof color. In other cases, such as the example shown in Figure 8B, these changes indicate complete re-development of a site. In this example from Boston, MA, a building with a dark roof is knocked down and replaced by a new building with a brighter roof. While there has essentially been no change in land cover, we see a dramatic shift in TCB in both the sequential date and DOY plots that is indicative of the change in impervious surface condition.

Time series can also capture abrupt changes in surface water conditions. For example Figure 8C shows a TCG time series for a coastal sand plain pond at the Ashumet Holly Wildlife Sanctuary (East Falmouth, MA) that would previously 'draw down' each summer, resulting in seasonal shifts between vegetated and non-vegetated states. Over the last two decades, sanctuary staff have observed a loss of this seasonal cycle, resulting in a persistent open water condition that has threatened the survival of a transient biota that includes numerous rare, threatened and endangered species. The TCG time series clearly captures the shift between vegetated and open water states, providing key data on both the location and timing of this abrupt change.

Disturbance and recovery

While regime shifts suggest a persistent change in ecosystem state, ecosystems also have some capacity to recover from disturbance (Holling 1973; Peterson et al. 1998). Disturbance-recovery trajectories can be conceptualized as the combination of two distinct functions: a step function, capturing an abrupt shift in state caused by a short-term event, such as a fire, flood or storm, followed by a period of recovery where the ecosystem asymptotically approaches the original or a new metastable state (Kennedy et al. 2014). Unlike sustained abrupt changes, which exhibit two or more distinct seasonal profiles, seasonal profiles of recovery trajectories show gradual mixing between states.

Many Landsat time series studies have examined trajectories of forest recovery (e.g. Viedma et al. 1997; Jin and Sader 2005; Kennedy et al. 2007; Masek et al. 2008), yet utilizing all high-quality observations can yield new insights into the nature and rate of recovery processes. For example Figure 9A shows TCG and TCW trajectories and seasonal profiles for a site that was cleared in the mid-1990s to presumably make way for a development along a previously constructed road. The initial clearing event, captured by GE imagery, causes a rapid decline in the overall magnitude and seasonal variability in TCG. In the following years, high-resolution images show the patch transitioning through various stages of succession, resulting in a gradual increase in the amplitude of TCG, as well as increased variability in TCW. The observed patterns in TCG and TCW can be used to monitor the rate of recovery in support of studies of forest successional and gap-phase dynamics.

Successional changes also occur in wetland ecosystems, and there is growing interest in time series analysis of wetland dynamics (e.g. Kayastha et al. 2012; Fickas et al. 2015). In temperate regions, rebounding beaver populations have a significant impact on wetland hydrology and vegetation (e.g. Naiman et al. 1988). The TCG and TCW time series shown in Figure 9B capture a typical sequence of wetland transitions resulting from beaver activity at the Wachusett Meadow Wildlife Sanctuary (Princeton, MA). According to sanctuary records, a beaver dam raised the

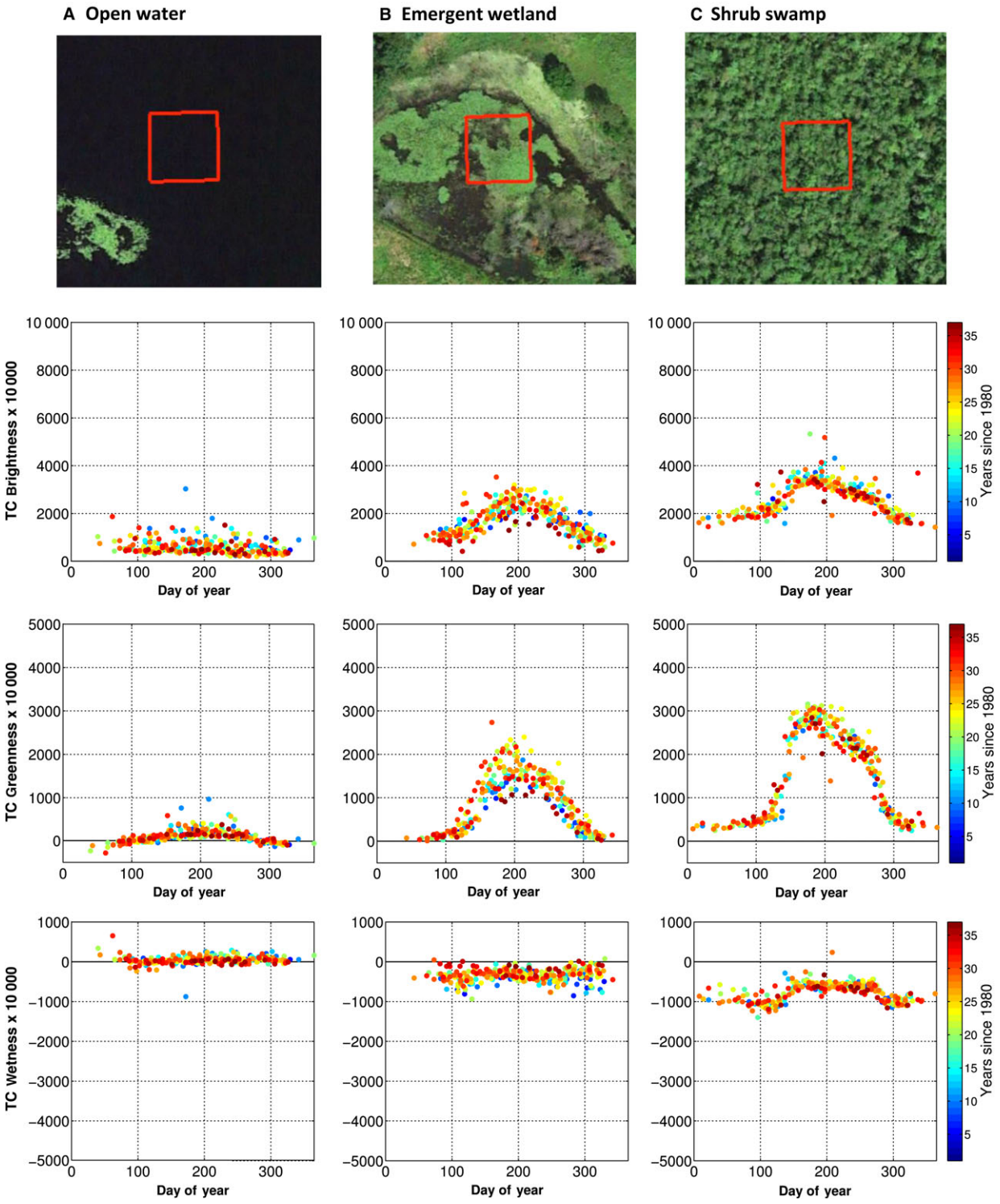

Figure 5. Tasseled Cap Brightness, Greenness and Wetness profiles for three examples along simple wetland gradient (WRS2 Path 12/Row 31). Plots show all available high-quality observations for a single pixel. A high-resolution Google Earth image of each site is included for reference, with the pixel footprint shown in red. Note variations in both overall magnitude and seasonal amplitude across the three TC components.

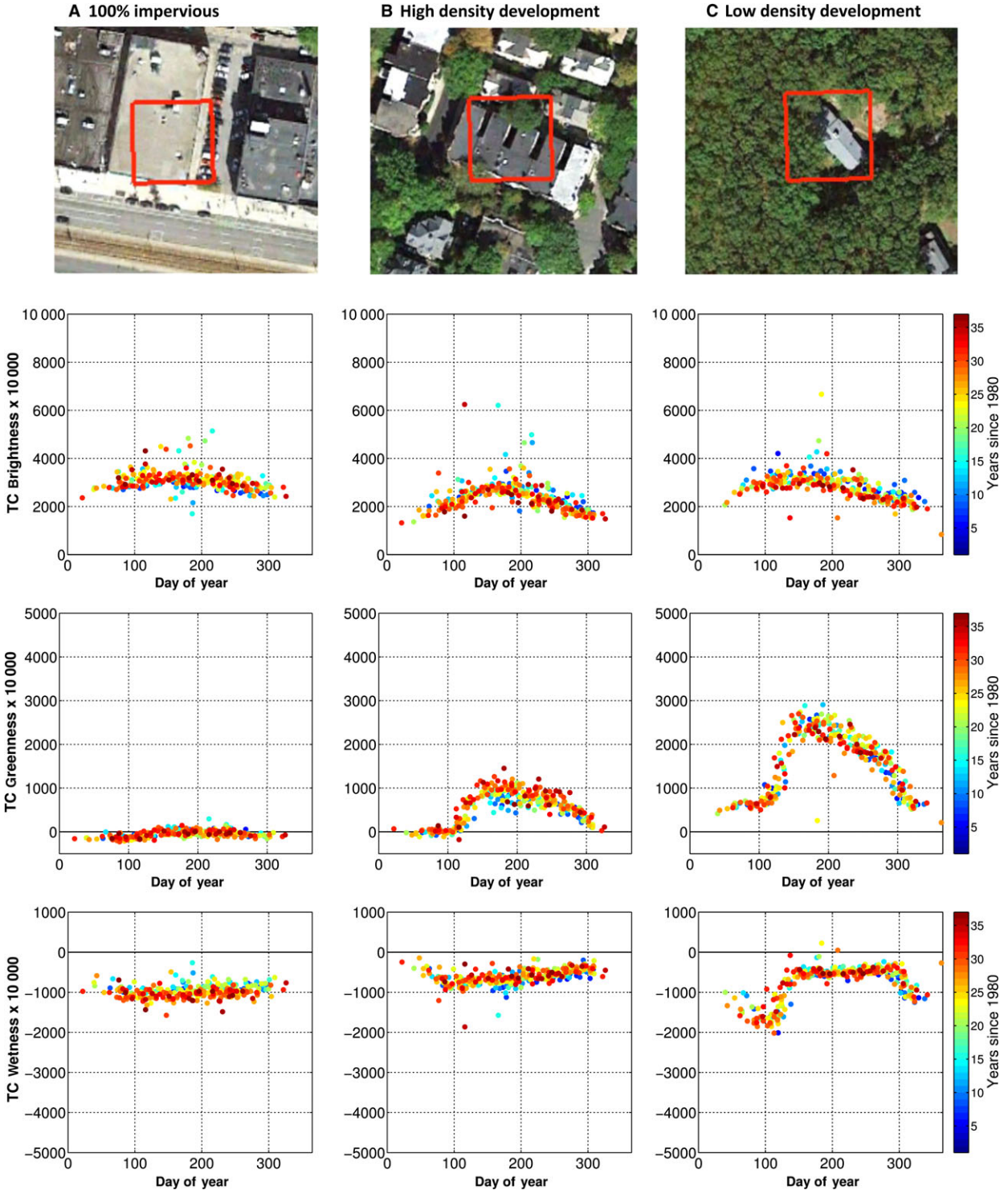

Figure 6. Tasseled Cap Brightness, Greenness and Wetness profiles for three examples along simple urban gradient (WRS2 Path 12/Row 31). Plots show all available high-quality observations for a single pixel. A high-resolution Google Earth image of each site is included for reference, with the pixel footprint shown in red. Note variations in both overall magnitude and seasonal amplitude across the three TC components.

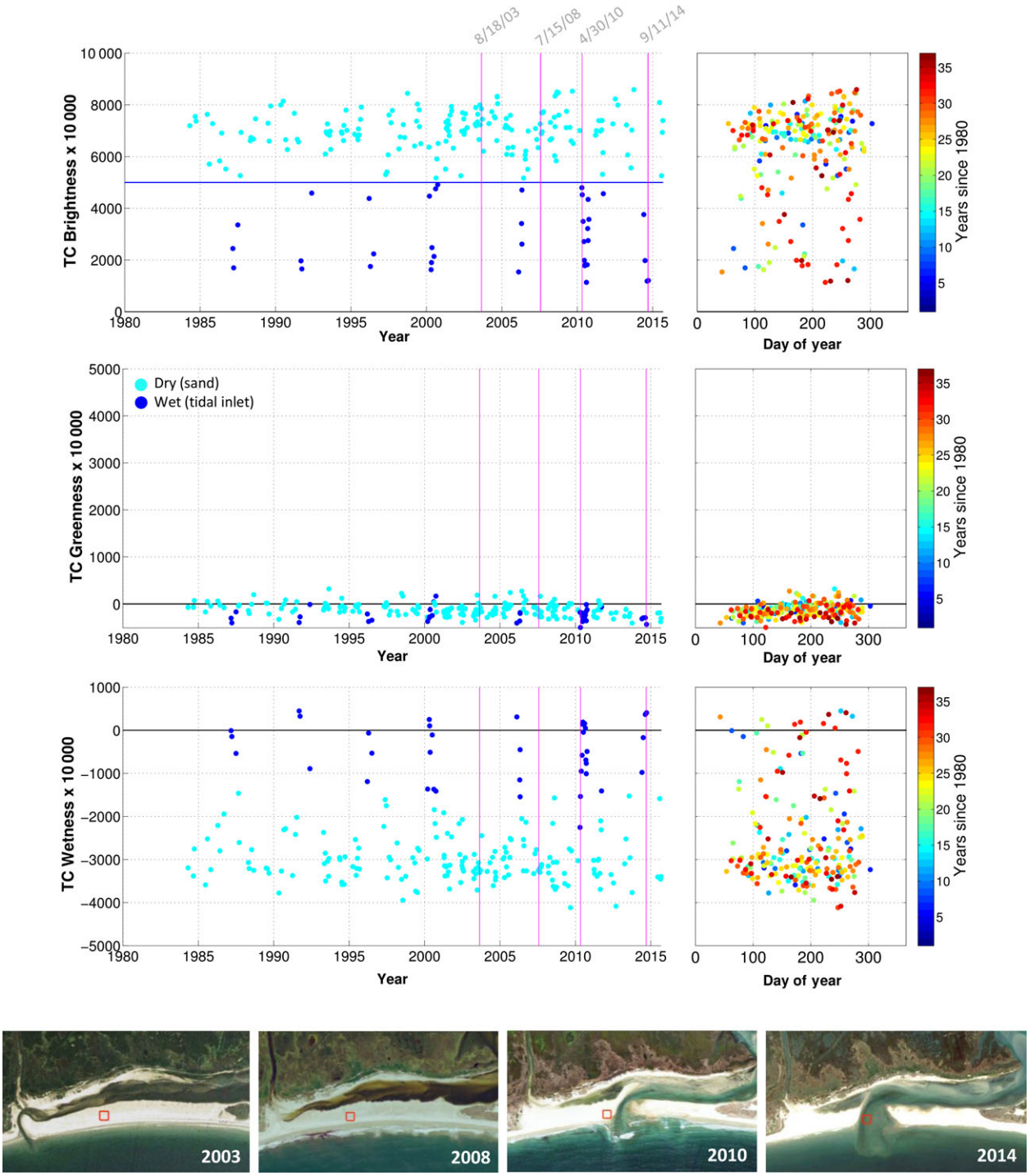

Figure 7. Cyclic trajectory of Allens Pond tidal inlet (WRS2 Path 12/Row 31). To roughly distinguish between sand and water conditions in sequential date plots, observations where Tasseled Cap Brightness (TCB) > 0.5 (50%) are shown in cyan, whereas observations where TCB < 0.5 are shown in blue. Vertical lines on sequential date plots correspond to dates of high-resolution Google Earth imagery (bottom). Note the different patterns of cyclic change across different Tasseled Cap components, particularly the lack of change in Tasseled Cap Greenness, as well as the short duration of the cyclic change events.

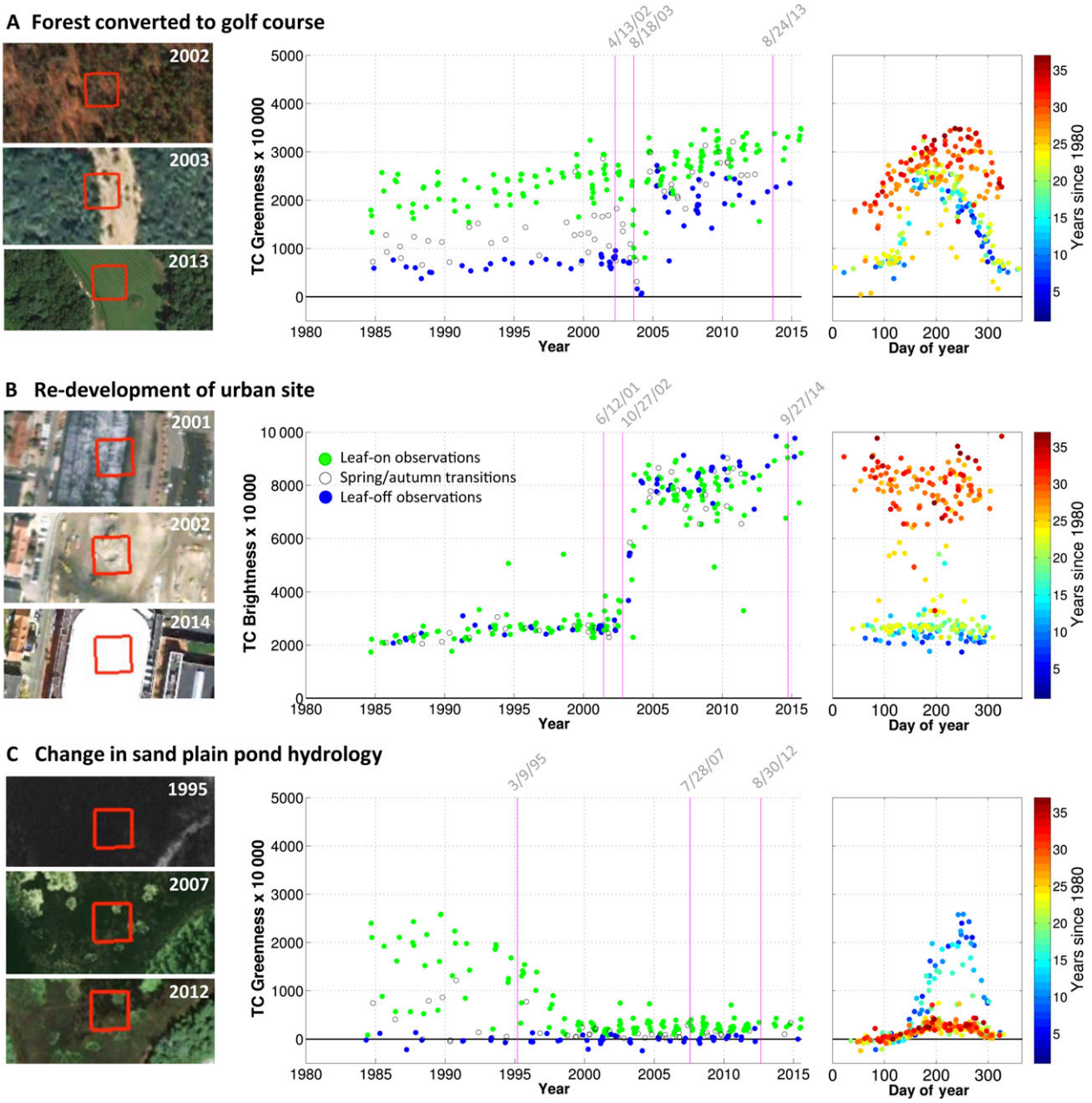

Figure 8. Examples of abrupt changes in Tasseled Cap Greenness for three sites (WRS2 Path 12/Row 31). Time series (A) captures an abrupt shift from forest cover to golf course. Time series (B) shows a change in impervious surface cover when a building is torn down and another re-built in its place. Time series (C) shows changes in the seasonal cycle of a coastal sand plain pond that has ceased 'drawing down' each summer. Vertical lines on sequential date plots correspond to dates of high-resolution Google Earth imagery (left). Note the clear step-like function in the sequential observations, as well as the distinct seasonal profiles in the DOY plots.

water level in a large red maple swamp around 1993, resulting in the mass die-off of woody vegetation, which is captured in the time series as a notable decrease in the amplitude of TCG. Following the flood event, marsh vegetation eventually re-colonized, as indicated by the gradual return of seasonal vegetation cycles in TCG and TCW. Interestingly, this particular wetland also experienced a dam breach around 2008. This second disturbance event is more readily seen in the TCW trajectory, confirming the different spectral bands are better suited for capturing different change processes. This example also illustrates the complexity of disturbance-recovery

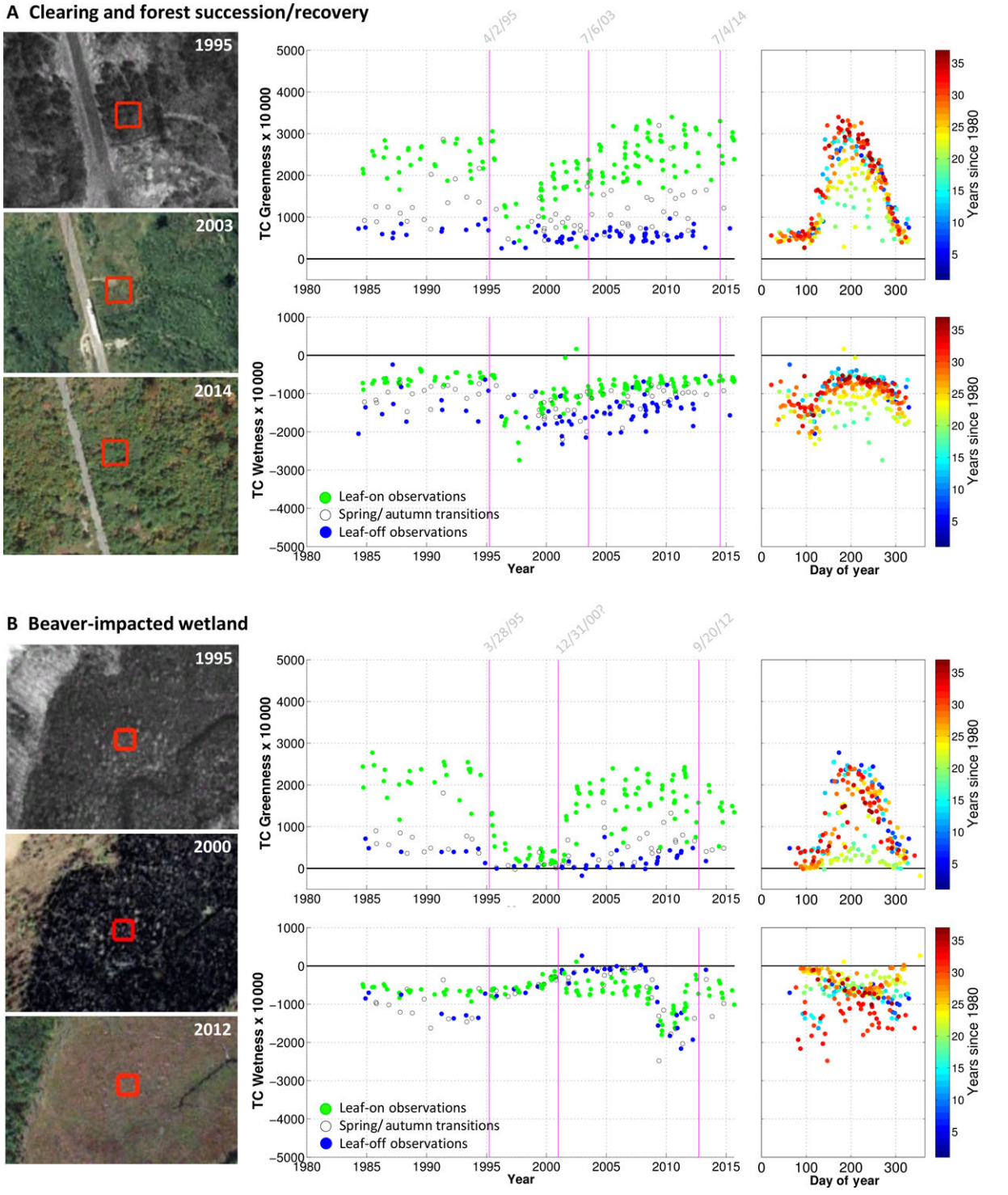

Figure 9. Examples of Tasseled Cap Greenness and Tasseled Cap Wetness disturbance-recovery trajectories for two sites (WRS2 Path 12/Row 31). Time series (A) captures the clearing and recovery of a forested area that appears to have been previously slated for development, whereas time series (B) captures the flooding and recovery of a wetland impacted by beavers. Vertical lines on sequential date plots correspond to dates of high-resolution Google Earth imagery (left). Note the different trajectories observed in different seasons and in different TC components, as well as the blending of seasonal profiles due to more gradual recovery processes after the initial abrupt change.

trajectories, especially where multiple disturbance events occur.

Gradual changes in state

Unlike abrupt changes and disturbance-recovery trajectories, which both rely on a step function to capture rapid shifts in ecosystem condition, gradual changes imply a trend function with no definitive break point–a slow shift from one state to another (Kennedy et al. 2014).

When an abrupt change occurs before the first time series observation, the temporal trajectory may only capture gradual recovery processes. For example Figure 10A captures a gradual transition from a mowed area to an

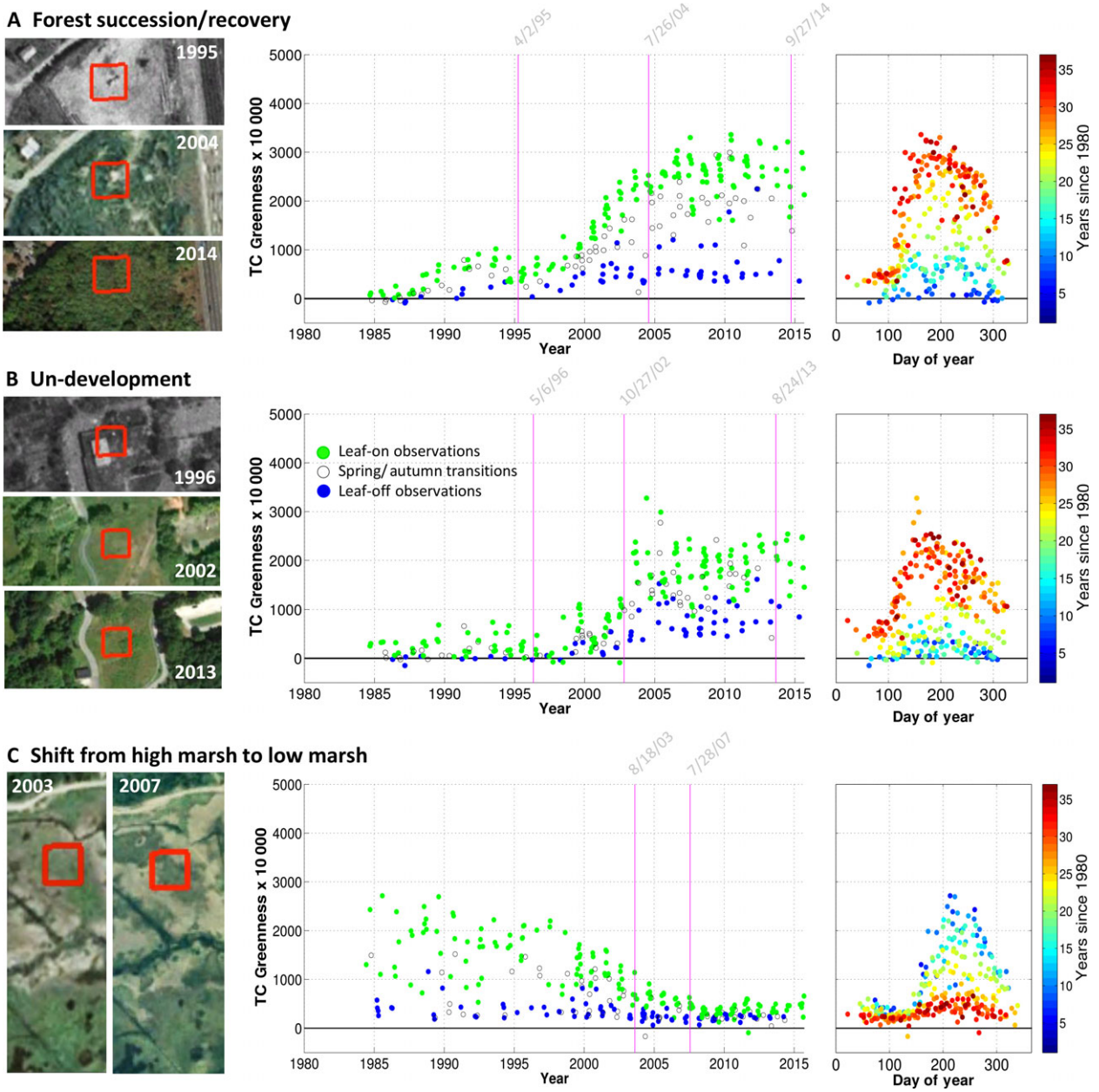

Figure 10. Examples of Tasseled Cap Greenness gradual change trajectories for three sites. Time series (A) (WRS2 Path 12/Row 31) captures recovery of a formerly managed grassy area to young forest. Time series (B) (WRS2 Path 12/Row 31) captures the recovery of herbaceous vegetation following the removal of a building. Time series (C) (WRS2 Path 11/Row 31) captures the response of marsh vegetation to sea level rise. Vertical lines on sequential date plots correspond to dates of high-resolution Google Earth imagery (left). Note the differences in directionality of change (recovery versus stress), as well as differences in the rates of change across sites/change processes.

early successional forest. An initial clearing event has occurred sometime in the past, but at the start of the time series, GE imagery suggests a managed herbaceous state. Over time, this patch moves through stages of succession, indicated by a gradual increase in the seasonal variability in TCG as woody vegetation re-established.

We have also observed a similar sort of gradual recovery trajectory in cases where human infrastructure has been removed and the site has been recolonized by vegetation. For example Figure 10B shows a TCG time series capturing a transition from impervious surface to bare ground to herbaceous vegetation after a building was removed at the Boston Nature Center, which sits on the grounds of the former Boston State Hospital. Here we see increases in both growing season and non-growing season TCG, as well as an overall trend toward increasing seasonal variability as vegetation re-established.

In other examples of gradual change, long-term changes in environmental conditions lead to a slow transition from one state to another with no history of abrupt disturbance. Figure 10C shows the TCG trajectory for a coastal salt marsh on Cape Cod affected by sea level rise. While Smith (2015) documented areas of this marsh that had and had not changed between 1984 and 2013, time series data from this Middle Meadow site show a gradual decrease in the seasonal variability in TCG over time, providing greater insight into both the timing and rate of change. By comparing rates of change across sites, it becomes possible to quantify not only the overall impacts of sea level rise across large areas, but also to test hypotheses regarding the long-term dynamics and resilience of impacted ecosystems.

Discussion

The Landsat legacy of single-date image classifications and before-after change detection has historically limited our ability to connect multi-spectral Earth observations to complex ecosystem processes and landscape dynamics (Kennedy et al. 2014). Now that we can look back across the complete record of Landsat observations, we are able to map and monitor the past and present conditions of ecosystems around the world, to test ecological theories at scales from local to global, and to model landscape change as the conceptually simple, but mathematically complex process that it really is. The examples presented here showcase how the full temporal dimension of the Landsat archive can be used to further the study of land cover characterization, ecosystem phenology and landscape dynamics. These examples also emphasize the importance of understanding not only the seasonal and change signals, but also interacting processes driving variability in these signals over time and across sites.

Our exploratory work on seasonal profiles, which builds on previous Landsat-based studies of phenology (Fisher et al. 2006; Melaas et al. 2013), suggests there is still much to learn about intra-annual patterns of reflectance in relatively stable ecosystems. In our forest examples, we observed notable differences in mean annual reflectance, seasonal variability and growing season length. A more comprehensive and robust library of spectral-temporal reference examples, akin to the libraries of spectra created for hyperspectral analysis (e.g. Price 1994; Zomer et al. 2009), would make it possible to conduct a more thorough investigation of variability in spectral-temporal properties across different forest types at local, regional and global scales. Such work could also be extended to include discrimination of non-forest cover types. Dry season phenology metrics derived from Landsat time series have been used to improve separability of grass-dominated and woody pastures (Rufin et al. 2015), and based on the examples presented here, we expect that spectral-temporal information will aid in improved mapping of other notoriously difficult classes such as wetland types and gradients of urban development. Time series data have also recently been used to map sub-pixel surface water area (Halabisky et al. 2016), and our examples of emergent wetland and low-density residential cover types further support the potential utility of seasonal profiles for mixture modeling. Still, many questions remain regarding the variability in spectral-temporal properties across cover types as well as the drivers of seasonal change, including sun and sensor geometry, vegetation structure and moisture conditions.

In reviewing examples of inter-annual change, we observed that time series of all available high-quality Landsat data consistently reveal complex underlying processes that would be difficult to assess using bi-temporal or even annual change detection approaches. While annual trajectories have proven useful for quantifying the timing and magnitude of abrupt disturbances, particularly in forested ecosystems (e.g. Huang et al. 2010; Kennedy et al. 2010), more subtle change process, such as post-disturbance recovery and changes in condition are better captured using denser time series (e.g. DeVries et al. 2015b; Rufin et al. 2015). By increasing the frequency of observations, we are able to discern a greater variety of landscape processes, including cyclic and gradual change processes that could easily be mischaracterized or missed altogether if a more sparse set of observations were used. Furthermore, our work highlights the importance of multi-spectral observations in detecting change processes. Many time series studies to date have been univariate, considering time series of a single spectral band or index (e.g. Meigs et al. 2011; DeVries et al. 2015b), but we find that that both seasonal patterns and change processes

manifest differently in different spectral bands and indices.

Our hand-picked examples clearly demonstrate that with increased frequency of Landsat observations, it becomes possible to characterize seasonal dynamics and to detect major and minor disturbances in ecosystem condition. Yet the ability to detect and interpret seasonal cycles and land cover change depends on the availability of both Landsat imagery and suitable reference information. The number of available images, as well as the number of clear observations, can vary greatly across regions and even from scene to scene (Hansen and Loveland 2012; Kovalskyy and Roy 2013). While the vast majority of our examples were drawn from the US, where the Landsat record is relatively complete, geographic and temporal coverage of Landsat data can be far more uneven in other parts of the world.

When entire years of imagery are missing from the USGS archive, as observed in time series data from Finland, Colombia and Vietnam, trajectory-based analysis can be problematic, with large gaps between acquisitions potentially obscuring the timing of change events. In these places, time series analysis will likely benefit from the Landsat Global Archive Consolidation effort (Wulder et al. 2015), which continues to integrate previously unavailable Landsat imagery into the USGS holdings from many international receiving stations. From the perspective of seasonal signatures, a more difficult challenge is the loss of data due to clouds and snow. Forest profiles from Colombia exhibit data gaps during the April and October rainy seasons, and examples from Finland show that there are practically no clear snow-free observations during the winter months (November through March) (Figs. 3 and 4). In tropical regions, such seasonal gaps may not have a dramatic impact on assessing intra-annual signatures, as forest conditions are relatively consistent throughout the year, but at more northern latitudes where vegetation exhibits stronger seasonality, missing observations can obscure the shape of the full spectral-temporal profile. High latitude image overlap zones can be used to increase the number of available observations (e.g. Ju and Masek 2016; Sulla-Menashe et al. 2016), but in many cases, seasonal and periodic gaps in time series coverage will persist and analysis approaches will need to be adapted accordingly.

Beyond limitations of data availability, the utility of time series information is directly linked with our ability to interpret the observed time series signals and the ecological processes and interactions they capture. While GE provides a ready source of historical high-resolution imagery, the quantity, quality and timing of available images can vary significantly. We find GE imagery useful for identifying the condition of a pixel at a single point in time or validating that an abrupt change has occurred, but interpreting more complex seasonal signals and disturbance patterns often requires more specialized expertise on site-specific ecosystem conditions, long-term dynamics and drivers of change. Thus, progress in the use of remotely sensed time series for the study of ecological landscape dynamics will be highly contingent upon the ability to interpret time series data using existing ecological datasets and local ecological knowledge, and to extrapolate lessons learned at data-rich locations to the larger landscape using automated approaches that capture spatial and temporal variability in time series data (Kennedy et al. 2014; DeVries et al. 2016).

Landsat is currently one of the most cost-effective sources of information on ecosystem extent, status, trends and responses to stressors over large areas (Rose et al. 2014), and the opportunities for ecosystem mapping, monitoring and comparative ecology using all available Landsat observations extend far beyond what has been presented here. Since the opening of the Landsat archive in 2008, we have only just begun to understand the power of using all available Landsat imagery for the study of ecology. With increasing availability of moderate resolution optical imagery (Turner et al. 2015), time series-based approaches to ecosystem mapping and monitoring are becoming more common and more powerful. It is our hope that the examples presented in this study will serve to further facilitate the current shift toward an ecological view of change (Kennedy et al. 2014), and will encourage future work on quantifying and analyzing relationships between time series data, ecosystems and ecological processes.

Acknowledgments

This work was funded in part by US Forest Service Grant 13-CR-11221638-146, US Geological Survey Grant G12PC00070, NASA Grant NNX13AP42, and the Boston University Pardee Center for the Longer-Range Future. The content of this document does not necessarily represent the views or policies of the Department of the Interior, nor does mention of trade names, commercial products or organizations imply endorsement by the U.S. Government. We would like to acknowledge and thank the many individuals who contributed to our examples database, including Robert Buchsbaum, Jeff Collins, Tom Lautzenheiser, Elissa Landre, and Cindy Dunn of the Massachusetts Audubon Society; Brian Hawthorne of the Massachusetts Division of Fisheries and Wildlife; Matthieu Molinier of VTT Earth Observation; Ilkka Korpela and Pekka Kaitaniemi of Helsinki University; and Sergio Fagherazzi and Paulo Arevalo of Boston University. We also thank Marta Ribera and two anonymous reviewers for their insightful comments on the content, style and organization of this manuscript.

Data Accessibility

All data and code used to produce the figures in this publication can be accessed at https://github.com/valpasq/2016_ImageryEcology, doi:10.5281/zenodo.46265. This repository also hosts KML files for each pixel to facilitate review of high-resolution GE imagery for each example site.

References

Adam, E., O. Mutanga, and D. Rugege. 2009. Multispectral and hyperspectral remote sensing for identification and mapping of wetland vegetation: a review. *Wetlands Ecol. Manage.* **18**, 281–296. doi:10.1007/s11273-009-9169-z).

Brooks, E. B., R. H. Wynne, V. A. Thomas, C. E. Blinn, and J. W. Coulston. 2014. On-the-Fly massively multitemporal change detection using statistical quality control charts and Landsat data. *IEEE Trans. Geosci. Remote Sens.* **52**, 3316–3332. doi:10.1109/TGRS.2013.2272545.

Cadenasso, M. L., S. T. A. Pickett, and K. Schwarz. 2007. Spatial heterogeneity in urban ecosystems: reconceptualizing land cover and a framework for classification. *Front. Ecol. Environ.* **5**, 80–88. doi:10.1890/1540-9295(2007) 5[80:SHIUER]2.0.CO;2.

Cihlar, J. 2000. Land cover mapping of large areas from satellites: status and research priorities. *Int. J. Remote Sens.* **21**, 1093–1114. doi:10.1080/014311600210092.

Cohen, W. B., and S. N. Goward. 2004. Landsat's role in ecological applications of remote sensing. *Bioscience* **54**, 535. doi:10.1641/0006-3568(2004) 054[0535:LRIEAO]2.0.CO;2.

Cohen, W. B., and T. A. Spies. 1992. Estimating structural attributes of Douglas-fir/western hemlock forest stands from Landsat and SPOT imagery. *Remote Sens. Environ.* **41**, 1–17. doi:10.1016/0034-4257(92)90056-P.

Cohen, W. B., T. K. Maiersperger, T. A. Spies, and D. R. Oetter. 2001. Modelling forest cover attributes as continuous variables in a regional context with Thematic Mapper data. *Int. J. Remote Sens.* **22**, 2279–2310. doi:10.1080/01431160121472.

Coppin, P., I. Jonckheere, K. Nackaerts, B. Muys, and E. Lambin 2004. Digital change detection methods in ecosystem monitoring: a review. *Int. J. Remote Sens.* **25**, 1565–1596. doi:10.1080/0143116031000101675.

Cowardin, L. M., and V. I. Myers. 1974. Remote sensing for identification and classification of wetland vegetation. *J. Wildl. Manag.* **38**, 308–314.

Crist, E. P. 1985. A TM Tasseled Cap equivalent transformation for reflectance factor data. *Remote Sens. Environ.* **17**, 301–306. doi:10.1016/0034-4257(85)90102-6.

Crist, E. P., and R. C. Cicone. 1984. A physically-based transformation of Thematic Mapper data—The TM Tasseled Cap. *IEEE Trans. Geosci. Remote Sens.*, GE-22 **3**, 256–263. doi:10.1109/TGRS.1984.350619.

Crist, E. P., and R. J. Kauth. 1986. The Tasseled Cap demystified. *Photogramm. Eng. Remote Sensing* **52**, 81–86.

Dall'Olmo, G., and A. Karnieli. 2002. Monitoring phenological cycles of desert ecosystems using NDVI and LST data derived from NOAA-AVHRR imagery. *Int. J. Remote Sens.* **23**, 4055–4071. doi:10.1080/01431160110115988

DeVries, B., J. Verbesselt, L. Kooistra, and M. Herold. 2015a. Robust monitoring of small-scale forest disturbances in a tropical montane forest using Landsat time series. *Remote Sens. Environ.* **161**, 107–121. doi:10.1016/j.rse.2015.02.012.

DeVries, B., M. Decuyper, J. Verbesselt, A. Zeileis, M. Herold, and S. Joseph. 2015b. Tracking disturbance-regrowth dynamics in tropical forests using structural change detection and Landsat time series. *Remote Sens. Environ.* **169**, 320–334.

DeVries, B., A. K. Pratihast, J. Verbesselt, L. Kooistra, and M. Herold. 2016. Characterizing forest change using community-based monitoring data and Landsat time series. *PLoS One* **11**, e0147121. doi:10.1371/journal.pone.0147121.

Dymond, C. C., D. J. Mladenoff, and V. C. Radeloff. 2002. Phenological differences in Tasseled Cap indices improve deciduous forest classification. *Remote Sens. Environ.* **80**, 460–472. doi:10.1016/S0034-4257(01)00324-8.

Fickas, K. C., W. B. Cohen, and Z. Yang. 2015. Landsat-based monitoring of annual wetland change in the Willamette Valley of Oregon, USA from 1972 to 2012. *Wetlands Ecol. Manage.*, 1–21. doi:10.1007/s11273-015-9452-0.

Fisher, J., J. Mustard, and M. Vadeboncoeur. 2006. Green leaf phenology at Landsat resolution: scaling from the field to the satellite. *Remote Sens. Environ.* **100**, 265–279. doi:10.1016/j.rse.2005.10.022.

FitzGerald, D. M., I. V. Buynevich, R. A. Davis, and M. S. Fenster. 2002. New England tidal inlets with special reference to riverine-associated inlet systems. *Geomorphology* **48**, 179–208. doi:10.1016/S0169-555X(02)00181-2.

Folke, C., S. Carpenter, B. Walker, M. Scheffer, T. Elmqvist, L. Gunderson, and C. S. Holling, 2004. Regime shifts, resilience, and biodiversity in ecosystem management. *Annu. Rev. Ecol. Evol. Syst.* **35**, 557–581.

Gómez, C., J. C. White, and M. A. Wulder. 2016. Optical remotely sensed time series data for land cover classification: a review. *ISPRS J. Photogramm. Remote Sens.* **116**, 55–72. doi:10.1016/j.isprsjprs.2016.03.008.

Halabisky, M., L. M. Moskal, A. Gillespie, and M. Hannam. 2016. Reconstructing semi-arid wetland surface water dynamics through spectral mixture analysis of a time series of Landsat satellite images (1984–2011). *Remote Sens. Environ.* **177**, 171–183. doi:10.1016/j.rse.2016.02.040.

Hansen, M. C., and T. R. Loveland. 2012. A review of large area monitoring of land cover change using Landsat data.

Remote Sens. Environ. **122**, 66–74. doi:10.1016/j.rse.2011.08.024.

Hansen, M. C., P. V. Potapov, R. Moore, M. Hancher, S. A. Turubanova, A. Tyukavina, et al. 2013. High-resolution global maps of 21st-century forest cover change. *Science* **342**, 850–853. doi:10.1126/science.1244693.

Healey, S., W. Cohen, Y. Zhiqiang, and O. Krankina. 2005. Comparison of Tasseled Cap-based Landsat data structures for use in forest disturbance detection. *Remote Sens. Environ.* **97**, 301–310. doi:10.1016/j.rse.2005.05.009.

Hermosilla, T., M. A. Wulder, J. C. White, N. C. Coops, and G. W. Hobart. 2015. An integrated Landsat time series protocol for change detection and generation of annual gap-free surface reflectance composites. *Remote Sens. Environ.* **158**, 220–234. doi:10.1016/j.rse.2014.11.005.

Holling, C. S. 1973. Resilience and stability of ecological systems. *Annu. Rev. Ecol. Syst.* **4**, 1–23.

Huang, C., S. N. Goward, J. G. Masek, N. Thomas, Z. Zhu, and J. E. Vogelmann. 2010. An automated approach for reconstructing recent forest disturbance history using dense Landsat time series stacks. *Remote Sens. Environ.* **114**, 183–198. doi:10.1016/j.rse.2009.08.017.

Jensen, J. R., and D. C. Cowen. 1999. Remote sensing of urban/suburban infrastructure and socio-economic attributes. *Photogramm. Eng. Remote Sensing* **65**, 611–623. doi:10.1002/9780470979587.ch22.

Jin, S., and S. A. Sader. 2005. Comparison of time series Tasseled Cap wetness and the normalized difference moisture index in detecting forest disturbances. *Remote Sens. Environ.* **94**, 364–372. doi:10.1016/j.rse.2004.10.012.

Ju, J., and J. G. Masek. 2016. The vegetation greenness trend in Canada and US Alaska from 1984–2012 Landsat data. *Remote Sens. Environ.* **176**, 1–16. doi:10.1016/j.rse.2016.01.001.

Kayastha, N., V. Thomas, J. Galbraith, and A. Banskota. 2012. Monitoring wetland change using inter-annual Landsat time-series data. *Wetlands* **32**, 1149–1162. doi:10.1007/s13157-012-0345-1.

Kennedy, R. E., W. B. Cohen, and T. A. Schroeder. 2007. Trajectory-based change detection for automated characterization of forest disturbance dynamics. *Remote Sens. Environ.* **110**, 370–386. doi:10.1016/j.rse.2007.03.010.

Kennedy, R. E., Z. Yang, and W. B. Cohen. 2010. Detecting trends in forest disturbance and recovery using yearly Landsat time series: 1. LandTrendr–Temporal segmentation algorithms. *Remote Sens. Environ.* **114**, 2897–2910. doi:10.1016/j.rse.2010.07.008.

Kennedy, R. E., S. Andréfouët, W. B. Cohen, C. Gómez, P. Griffiths, M. Hais, et al. 2014. Bringing an ecological view of change to Landsat-based remote sensing. *Front. Ecol. Environ.* **12**, 339–346. doi:10.1890/130066.

Kim, D.-H., J. O. Sexton, P. Noojipady, C. Huang, A. Anand, S. Channan, et al. 2014. Global, Landsat-based forest-cover change from 1990 to 2000. *Remote Sens. Environ.* **155**, 178–193. doi:10.1016/j.rse.2014.08.017.

Kovalskyy, V., and D. P. Roy. 2013. The global availability of Landsat 5 TM and Landsat 7 ETM + land surface observations and implications for global 30 m Landsat data product generation. *Remote Sens. Environ.* **130**, 280–293. doi:10.1016/j.rse.2012.12.003.

Lauer, D. T., S. A. Morain, and V. V. Salomonson. 1997. The Landsat program: its origins, evolution, and impacts. *Photogramm. Eng. Remote Sensing* **63**, 831–838. doi:0099-1112I9716307-831$3.00/0.

Loveland, T. R., and J. L. Dwyer. 2012. Landsat: building a strong future. *Remote Sens. Environ.* **122**, 22–29. doi:10.1016/j.rse.2011.09.022.

Lu, D., and Q. Weng. 2005. Urban classification using full spectral information of Landsat ETM+ imagery in Marion County, Indiana. *Photogramm. Eng. Remote Sensing* **71**, 1275–1284.

Markham, B. L., and D. L. Helder. 2012. Forty-year calibrated record of earth-reflected radiance from Landsat: a review. *Remote Sens. Environ.* **122**, 30–40. doi:10.1016/j.rse.2011.06.026.

Masek, J. G., C. Huang, R. Wolfe, W. Cohen, F. Hall, J. Kutler, et al. 2008. North American forest disturbance mapped from a decadal Landsat record. *Remote Sens. Environ.* **112**, 2914–2926. doi:10.1016/j.rse.2008.02.010.

Meigs, G. W., R. E. Kennedy, and W. B. Cohen. 2011. A Landsat time series approach to characterize bark beetle and defoliator impacts on tree mortality and surface fuels in conifer forests. *Remote Sens. Environ.* **115**, 3707–3718. doi:10.1016/j.rse.2011.09.009.

Melaas, E. K., M. A. Friedl, and Z. Zhu. 2013. Detecting interannual variation in deciduous broadleaf forest phenology using Landsat TM/ETM+ data. *Remote Sens. Environ.* **132**, 176–185. doi:10.1016/j.rse.2013.01.011.

Naiman, R. J., C. A. Johnston, and J. C. Kelley. 1988. Alteration of North American streams by beaver. *BioScience.* **38**, 753–762. doi:10.2307/1310784.

Özesmi, S. L., and M. E. Bauer. 2002. Satellite remote sensing of wetlands. *Wetlands Ecol. Manage.* **10**, 381–402. doi:10.1023/A:1020908432489.

Peterson, G., C. R. Allen, and C. S. Holling. 1998. Ecological resilience, biodiversity, and scale. *Ecosystems* **1**, 6–18. doi:10.1007/s100219900002.

Price, J. C. 1994. How unique are spectral signatures? *Remote Sens. Environ.* **49**, 181–186.

Reese, H. M., T. M. Lillesand, D. E. Nagel, J. S. Stewart, R. A. Goldmann, T. E. Simmons, et al. 2002. Statewide land cover derived from multiseasonal Landsat TM data–A retrospective of the WISCLAND project. *Remote Sens. Environ.* **82**, 224–237. doi:10.1016/S0034-4257(02)00039-1.

Ridd, M. K. 1995. Exploring V-I-S (vegetation-impervious surface-soil) model for urban ecosystem analysis through

remote sensing: comparative anatomy for cities. *Int. J. Remote Sens.* **16**, 2165–2185. doi:10.1080/01431169508954549.

Rose, R. A., D. Byler, J. R. Eastman, E. Fleishman, G. Geller, S. Goetz, et al. 2014. Ten ways remote sensing can contribute to conservation. *Conserv. Biol.* **29**, 350–359. doi:10.1111/cobi.12397.

Rufin, P., H. Müller, D. Pflugmacher, and P. Hostert. 2015. Land use intensity trajectories on Amazonian pastures derived from Landsat time series. *Int. J. Appl. Earth Obs. Geoinf.* **41**, 1–10.

Smith, S. M. 2015. Vegetation change in salt marshes of Cape Cod National Seashore (Massachusetts, USA) between 1984 and 2013. *Wetlands* **35**, 127–136. doi:10.1007/s13157-014-0601-7.

Sulla-Menashe, D., M. A. Friedl, and C. E. Woodcock. 2016. Sources of bias and variability in long-term Landsat time series over Canadian boreal forests. *Remote Sens. Environ.* **177**, 206–219. doi:10.1016/j.rse.2016.02.041.

Turner, W., C. Rondinini, N. Pettorelli, B. Mora, A. K. Leidner, Z. Szantoi, et al. 2015. Free and open-access satellite data are key to biodiversity conservation. *Biol. Conserv.* **182**, 173–176. doi:10.1016/j.biocon.2014.11.048.

U.S. Geological Survey. 2015. Product guide: Landsat surface reflectance products courtesy of the U.S. Geological Survey, 1–27, Available at: http://landsat.usgs.gov/documents/cdr_sr_product_guide.pdf (accessed 8 May 2016).

Viedma, O., J. Melia, D. Segarra, and J. GarciaHaro. 1997. Modeling rates of ecosystem recovery after fires by using Landsat TM data. *Remote Sens. Environ.* **61**, 383–398. doi:10.1016/S0034-4257(97)00048-5.

Vogelmann, J. E., G. Xian, C. Homer, and B. Tolk. 2012. Monitoring gradual ecosystem change using Landsat time series analyses: case studies in selected forest and rangeland ecosystems. *Remote Sens. Environ.* **122**, 92–105. doi:10.1016/j.rse.2011.06.027.

Walsh, S. J. 1980. Coniferous tree species mapping using Landsat data. *Remote Sens. Environ.* **9**, 11–26. doi:10.1016/0034-4257(80)90044-9.

Wolter, P. T., D. J. Mladenoff, G. E. Host, and T. R. Crow. 1995. Improved forest classification in the Northern Lake-States using multitemporal landsat imagery. *Photogramm. Eng. Remote Sensing* **61**, 1129–1143.

Woodcock, C. E., et al. 2008. Free access to Landsat data. *Science* **320**, 1011. doi:10.1126/science.320.5879.1011a.

Wulder, M. A., J. C. White, S. N. Goward, J. G. Masek, J. R. Irons, M. Herold, et al. 2008. Landsat continuity: issues and opportunities for land cover monitoring. *Remote Sens. Environ.* **112**, 955–969.

Wulder, M. A., J. G. Masek, W. B. Cohen, T. R. Loveland, and C. E. Woodcock. 2012. Opening the archive: how free data has enabled the science and monitoring promise of Landsat. *Remote Sens. Environ.* **122**, 2–10. doi:10.1016/j.rse.2012.01.010.

Wulder, M. A., J. C. White, T. R. Loveland, C. E. Woodcock, A. S. Belward, and W. B. Cohen, et al. 2015. The global Landsat archive: Status, consolidation, and direction. *Remote Sens. Environ.* doi:10.1016/j.rse.2015.11.032

Zhu, Z., and C. E. Woodcock. 2014. Continuous change detection and classification of land cover using all available Landsat data. *Remote Sens. Environ.* **144**, 152–171.

Zhu, Z., C. E. Woodcock, J. Rogan, and J. Kellndorfer. 2012a. Assessment of spectral, polarimetric, temporal, and spatial dimensions for urban and peri-urban land cover classification using Landsat and SAR data. *Remote Sens. Environ.* **117**, 72–82. doi:10.1016/j.rse.2011.07.020.

Zhu, Z., C. E. Woodcock, and P. Olofsson. 2012b. Continuous monitoring of forest disturbance using all available Landsat imagery. *Remote Sens. Environ.* **122**, 75–91. doi:10.1016/j.rse.2011.10.030.

Zomer, R. J., A. Trabucco, and S. L. Ustin. 2009. Building spectral libraries for wetlands land cover classification and hyperspectral remote sensing. *J. Environ. Manage.* **90**, 2170–2177. doi:10.1016/j.jenvman.2007.06.028.

